Simulation and analysis of InP/GaInP nanowire Esaki diodes for photovoltaic device applications

ODD RESTAD

SUPERVISED BY PROF. MAGNUS BORGSTRÖM AND DR. PYRY KIVISAARI

LUND UNIVERSITY
DIVISION OF SOLID STATE PHYSICS

June 2017

LUND UNIVERSITY

Abstract

In this thesis the WKB-approximation is used to simulate the tunneling current for an Esaki nanowire diode and the result is compared to data from Esaki nanowire diodes grown with MOVPE. The WKB-approximation with triangular potential barrier predicts a strong increase of the tunneling current as a function of the doping densities and at the highest doping levels it gives lower tunneling distances than more reliable drift-diffusion simulations and is thus overestimating the current. The voltage corresponding to the peak current was found to be much higher in the measured samples than in the simulations, and it is shown that an added contact resistance cannot explain this behaviour. Band tailing is suggested as a possible explanation for the difference in the voltage between simulations and experiments.

The diode characteristics of the Esaki diode samples are also studied at larger voltages. It is shown that an exponential current law fits well with the diode current at the larger voltages and the resulting contact resistance is too small to significantly change the tunnel current due to its low magnitude. An ideality factor was calculated from the fittings to be larger than 2 indicating that the excess current of the Esaki diode may be due to trap tunneling.

Acknowledgements

I would like to thank my supervisors Magnus Borgström and Pyry Kivisaari for their help and providing me with the comsol models used in this thesis. I would also like to thank Gaute Otnes for sharing data from nanowire Esaki diode measurements and Xulu Zeng for growing the nanowires.

Contents

1 Introduction **1**
1.1 Background . . . 1
1.2 Objectives and scope . . . 1
1.3 Scientific background . . . 1
1.3.1 Semiconductors . . . 1
1.3.2 Doping in semiconductors . . . 3
1.3.3 pn-junctions . . . 3
1.3.4 Esaki-diodes . . . 5
1.3.5 Solar cells . . . 6
1.3.6 Nanowire solar cells . . . 7
1.3.7 Tandem solar cells . . . 7
1.3.8 npin-structures with an Esaki diode . . . 8

2 Theory and Methods **9**
2.1 WKB-approximation . . . 9
2.2 Drift-Diffusion model . . . 12
2.3 Current transport in pn-junctions . . . 13
2.4 Band tailing . . . 14
2.5 Uncertainties in the tunneling model . . . 14
2.6 Nanowire growth . . . 15

3 Results and Discussion **16**
3.1 Current simulated with WKB-approximation . . . 16
3.2 Measured tunneling IV characteristics . . . 18
3.3 Tunneling current with contact resistance and band tailing . . . 19
3.4 Measured diode IV characteristics . . . 20
3.5 Simulation of npin-structure . . . 21

4 Conclusions **23**

References **24**

Appendix A Contact resistance sweeps **26**

Appendix B Matlab code **30**

1 Introduction

1.1 Background

As the energy consumption is increasing, solar cells and other renewable energy sources are very important substitute to fossil fuel since fossil fuels cause negative effects on the environment such as emission of SO_2 and NO_x [1]. The combustion of fossil fuel also increases the CO_2 responsible for global warming [2].

Solar energy has great potential since the earth yearly receives 3.9×10^{24} J in electromagnetic waves from the sun [3] and the global energy consumption 2014 was 5.7×10^{20} J [4].

Nanowires give the possibility to manufacture solar cells with comparable efficiency to planar solar cells but with lower material cost [5]. Tandem solar cells can be grown in nanowires to increase the efficiency but then a better understanding of the Esaki diode contact between the cells is needed and that is the focus of this thesis.

1.2 Objectives and scope

In this thesis, a modeling tool is constructed and evaluated for InP/GaInP nanowire Esaki diodes that can be integrated to drift-diffusion based device simulations. This is important because a good electrical contact is needed between the cells in a tandem solar cell (Sec. 1.3.7). Theoretical framework is constructed using the WKB approximation, and the results are compared with empirical data from nanowire Esaki diodes. The empirical data is from InP/GaInP heterostructure and therefore the simulations are performed for these materials. Simulations of a npin-structure are also made to show how to integrate the model with drift-diffusion simulations and to see how well the model can be used in more complex structures.

1.3 Scientific background

1.3.1 Semiconductors

A semiconductor is as the name suggests a material between a conductor (metal) and an insulator. All crystalline solid materials have a valence band and a conduction band which form from the atoms' valence electron state and the empty higher states respectively as illustrated in Fig. 1. The material determines the energy difference between the conduction band and the valence band. If the valence band and conduction band have no energy separation (band gap) or are overlapping as in Fig. 1(a) the material is a metal. If there is a small band gap it is a semiconductor, and a if there is a large band gap it is called an insulator (Fig 1b,c). Semiconductors usually have a band gap of up to a couple of eV [6] i.e. InAs with band gap on 0.35 eV and GaP with 2.3 eV.

In an atom the lowest energy states fill up first and then higher and higher energy states are filled until there are no electrons left (first K-shell, then L-shells etc.). This works a somewhat similar way for semiconductors with the difference that the states are much closer together in a semiconductor, so close that they are approximated with a continuous band of free electron-like states whose energy has a continuous dependence on the electrons' crystal momentum (or k vector).

If a potential is applied over a semiconductor at low temperature, so that it has a full valence band and an empty conduction band, the electrons cannot change their direction (because all states with other directions are full) and therefore there will be no current through the material. The semiconductor will under this condition work as an insulator. On the other hand if the

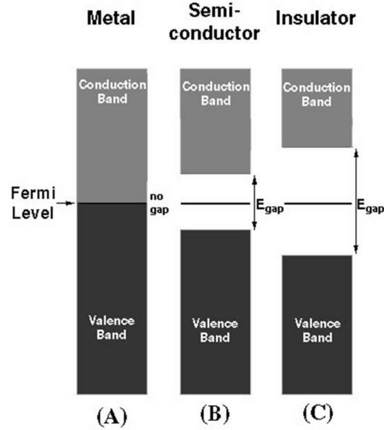

Figure 1: Schematic band diagram for metal (A), semiconductor (B) and insulator (C) with Fermi level drawn in the middle. Reprinted from Ref. [7]

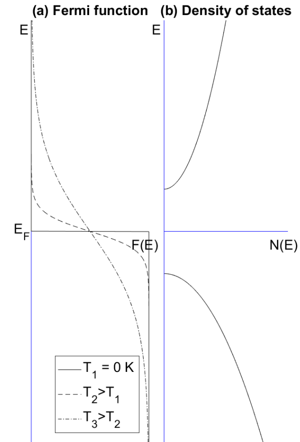

Figure 2: (a)Fermi function plotted for three different temperatures, and (b) the density of states plotted on the same energy scale

semiconductor is n-doped so that electrons are added to the empty conduction band (see Sec. 1.3.2), the conduction band will be partly filled and the electrons in the conduction band can change their direction when a potential is applied so that a net current can flow.

Electrons can be excited from the valence band to the conduction band by thermal energy, photons etc. and when the electrons get excited they leave an empty state in the valence band to fill a state in the conduction band. Electrons in the conduction band contribute to the current as explained in the previous paragraph. In addition the empty state in the valence band now allows for a change in electron velocity to align with the potential field. The empty states can mathematically be described as particles (called holes) with a positive charge. Semiconductors with as many electrons in the conduction band as there are holes in the valence band are referred to as intrinsic, in contrast to doped semiconductors (see Sec. 1.3.2 below).

Under thermal equilibrium the probability of a state being filled at an energy (E) is given by the Fermi function (Fig. 2 (a)):

$$F(E) = \frac{1}{1 + \exp((E - E_F)/k_B T)} \tag{1}$$

where k_B is the Boltzmann constant, T is the temperature and E_F is the Fermi level [8]. Therefore the probability of a state being filled at E_F is equal to 0.5 at a temperature above absolute zero. It is, however, frequently the case in semiconductors that there are no energy states available at the Fermi level as it is typically located inside the band gap. In the limit $T \to 0$, for $E < E_F$ then $F(E) \to 1$ and for $E > E_F$, $F(E) \to 0$. The probability a state is empty is $1 - F(E)$ and describes the hole concentration in the valence band.

Further the distribution of states is also important, because the Fermi function only describes the probability of a state to be occupied at energy E, not if there is a state at E. The density of states (DoS) for a three-dimensional crystal with isotropic parabolic energy bands is given by (Fig. 2(b)):

$$N(E) = \frac{\sqrt{2m^{*3}}}{\pi^2\hbar^3}\sqrt{E - E_C} \tag{2}$$

where m^* is the effective mass of the electrons and E_C is the energy at the edge of the conduction band [9]. The equation is also valid for holes in the conduction band if the electron effective mass is changed for the hole effective mass and $E - E_C$ is changed for $E_V - E$. The product of the Fermi function and the Density of states gives the density of occupied states. The number of charge carriers (n_e for electrons and n_h for holes) is then given by

$$n_e = \int_{E_C}^{\infty} N_e(E)F(E)dE \tag{3}$$

$$n_h = \int_{-\infty}^{E_V} N_h(E)(1 - F(E))dE \tag{4}$$

1.3.2 Doping in semiconductors

An important characteristic for semiconductors is the ability to dope them, i.e. create extra charge carriers in the conduction band or valence band. Doping is to replace a relatively small part of the atoms of the material with another element with a different number of valence electrons [6]. If the doping is very high so that the Fermi level is within the electron band the semiconductor is said to be degenerately doped.

For group IV semiconductors like silicon all atoms have four valence electrons. When an atom is replaced by a group III atom like Boron there will be one electron less in the valence band, a hole. Dopants with less valence electrons than the host material are called acceptors, and the semiconductor is said to be p-doped.

The other way a type IV semiconductor can be doped is with group V atoms like phosphorus. A group V atom has five valence atoms and thus a group V dopant will increase the number of electrons of the material. Dopants with extra electrons are called a donor atom, and the semiconductors is n-doped. The extra electrons will populate only part of the band and therefore they can carry a net current. As described in section 1.3.1 holes and electrons are charge carriers and therefore a doped semiconductor is usually more conducting better than an undoped semiconductor. For alloy semiconductors like InP the most effective dopants are typically other than group III or V elements, like zinc from group II, tin from group IV and sulphur from group VI in the case of InP [10]. Group IV elements can be either p- or n-doping depending on which atom it replaces.

1.3.3 pn-junctions

The pn-junction (diode) is a semiconductor structure where one side of the junction is p-doped and the other side is n-doped. This creates one side with more states empty of electrons (holes) in the valence band than in an intrinsic semiconductor and one side with excess electrons in the conduction band. In a pn-junction at thermal equilibrium, a region is depleted of free carriers which leaves part of the n-side (p-side) positively (negatively) charged due to the static ionized dopant atoms. These positive and negative ions constitute a nonzero net charge density close to the junction and create an electric field and therefore a potential difference. This leads to a band diagram as shown in figure 3. The region where the band is bending is called depletion region because it is almost depleted of free charge carriers (electrons and holes).

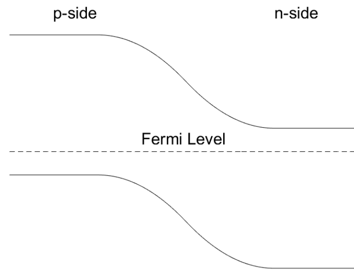

Figure 3: Band structure for a pn junction without any bias. Energy on the Y-axis and spacial coordinate on the X-axis

When an external potential (bias) is added so that the difference between the potential on the p- and n-side decreases it is called forward bias and when the difference increases it is called reverse bias. An external bias also drives the conduction and valence bands out of a common thermal equilibrium. However, they can still typically be described by separate thermal equilibria, in which they have separate Fermi distributions with position-dependent quasi-Fermi levels instead of a single position-independent Fermi level (Sec. 1.3.1).

An interesting property of the pn-junction is that when it is forward biased, the current increases exponentially, but for reverse bias the current remains very low. A diagram of current versus potential (IV-diagram) is shown in figure 4. The small current at reverse bias is due to the fact that at reverse bias, electrons need to flow from the p-side to the n-side. For electrons to travel from the p-side to the n-side the electrons need to get to where there is a change in potential that is close to the edge of the depletion region. They are then pulled by the potential difference (drift) and end up on the n-side. The limiting factor here is how many electrons that end up on the edge of the depletion region from the p-side. The density of electrons is very small at the p-side and almost independent of potential difference (there is a slight dependant due to the increased electrical field over the junction causing more electrons to drift with the electrical field). So increased reverse bias leads to almost no change in total current. This same reasoning applies for hole current from the n-side to the p-side.

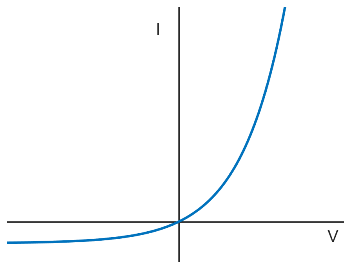

Figure 4: IV-characteristics for an ideal pn-junction.

At forward bias, on the other hand, electrons travel from the n-side to the p-side. There are many electrons on the n-side due to the doping and some of them have a high enough energy and the right direction to travel over to the p-side (diffusion). At forward bias the potential difference between the n- and p-side is decreased, which means that the potential barrier for electrons is also decreased. As described earlier the number of electrons at a certain energy is described by the Fermi-function and is exponentially decreasing with increased energy. The decrease of the potential barrier therefore means that when there is a forward bias the energy needed for an electron to travel to the p-side decreases and the number of electrons that have high enough energy increases exponentially. Again, the same reasoning applies for holes flowing from the p-side to the n-side.

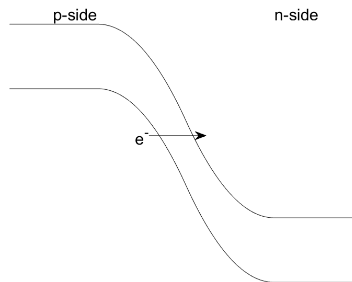

Figure 5: Schematic band structure of a heavily doped pn-junction under a large reverse applied bias.

As described (in the previous paragraphs) the current through a diode with reversed bias is almost unchanged, and this is true until a certain point called the reverse bias breakdown. When the breakdown point is reached there is a exponential increase in current. This can be due to two different factors called avalanche breakdown and Zener breakdown, the more relevant one for this thesis is the Zener breakdown (Shown in Fig. 5) since it occurs in high doped semiconductors. It happens when the diode has sufficient doping and reverse bias so the electrons can tunnel from the p-side to the n-side [11] (Fig. 5). Under Zener breakdown, even though there are no states for the electrons inside the band gap electrons can tunnel though the band gap and thereby flow to the other side as long as the tunnelling distance is short (usually of the order of nanometres). The extent of the depletion region decreases and the built-in electric field increases when doping levels increase which in the end leads to tunneling when the spatial extension of the junction is small enough and the electric field is high enough.

1.3.4 Esaki-diodes

The Esaki-diodes were first realized in a Germanium diode and explained by Leo Esaki [12]. The Esaki-diode is a pn-junction with high enough doping levels (around 10^{19} cm^{-3} or higher) so that the Fermi level is within the conduction and/or valence bands of the semiconductor, a situation commonly referred to as a degenerate semiconductor [8]. Figure 6 shows the band diagram for such a device. The heavy doping results in a possibility for the electrons to tunnel from the p-side to the n-side and vice versa similar to Zener breakdown but without applied bias. At zero bias there will be no net current since the tunnelling that can occur is equal on both sides. Fig. 6 (a) shows an

Esaki diode at zero bias. However, when a forward bias is applied to an Esaki-diode, there will be a an initial increase in current caused by an increasing number of electrons on the n-side that can tunnel to an empty state on the p-side (Fig. 6 (b)). But as the bias is increasing, the gap where tunnelling can occur will decrease causing a decrease in current until the bias gets large enough and the Esaki-diode works as a normal diode with no tunnelling [12] (Fig. 6 (c)). Additionally in this regime, some tunneling can take place through trap states inside the band gap, increasing the total current.

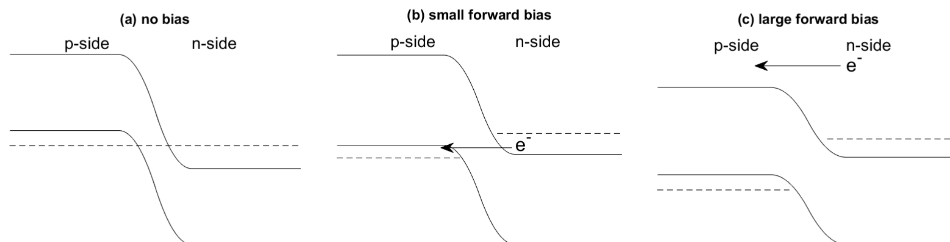

Figure 6: Esaki band structure for (a) no bias, (b) small bias and (c) larger bias. Dashed lines are the fermi level (a) and the quasi fermi levels (b and c).

1.3.5 Solar cells

When a photon is absorbed by a semiconductor, the photon transfers its energy to an electron that gets excited from the valence band to the conduction band of the semiconductor, creating an electron-hole pair. Electrons may then relax and recombine with a hole in the valence band emitting a photon (radiative recombination) or releasing their energy to the lattice heat (nonradiative recombination).

A solar cell is essentially a pn-junction contacted electrically from its both ends. When the electrons are excited within or close to the depletion region, the electron is pulled one way and the hole the opposite way thus separating them in space so they cannot recombine (Fig. 8). The electrons collected at the n-type contact and the holes collected at the p-type contact constitute the current generated by the solar cell.

To increase the collection of photogenerated charge carriers, an intrinsic (undoped) region can be added in solar cells between the n- and p-doped regions (creating a pin-structure). Due to the recombination processes that compete with the carrier collection by the contacts, typically only the electron-hole pairs that are generated within about one diffusion length of or in the depletion region contribute to the electric current by drifting with the electrical field. The insertion of an intrinsic region elongate the collection region by increasing the depletion region.

When a photon has lower energy than the band gap it is not possible for it to excite an electron over to the conduction band, and therefore no electrical current is produced. On the other hand if the photon has a higher energy than the band gap the electron will be excited into the conduction band but will then thermalise to the edge of the conduction band with energy lost as heat (phonons) [13]. Lower band gap thus results in more electrons absorbed but less energy gained for each electron. In 1961 Shockley and Queisser calculated the upper theoretical efficiency for a single pn-junction to 30 % with a band gap of 1.1 eV [14] given the solar spectrum.

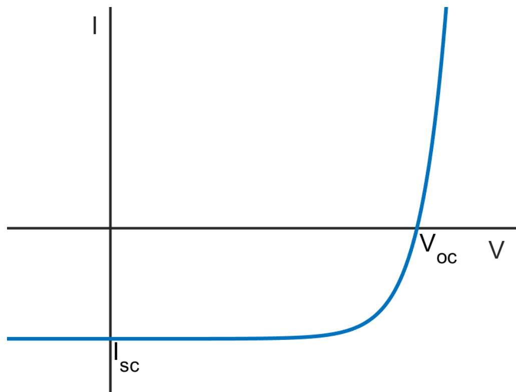

Figure 7: IV-characteristics of an illuminated solar cell. I_{sc} is the short circuit current and V_{oc} is the open circuit voltage.

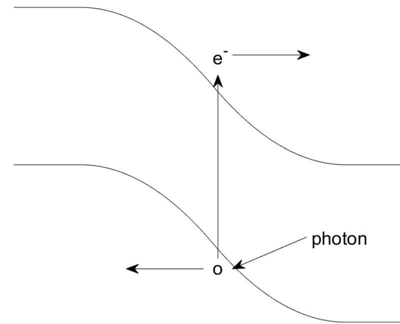

Figure 8: Excitation of an electron in a pn-junction.

1.3.6 Nanowire solar cells

Nanowire solar cells are like normal solar cells, but instead of using bulk material thin rods of the material are used instead. The wires are on the order of 10-1000 nm thick and typically have a separation of the order of 1 μm so nanowire solar cells have a possibility to use less material than planar solar cells. This can be an advantage particular if rare and expensive materials are used. While the simple and incomplete ray optics model yields absorption proportional to the surface coverage, in the case of nanowires wave resonance can increase the absorption per volume ratio by 20 [15], enabling nanowire array solar cells to absorb most of the incoming light even when the nanowires do not cover the whole surface. Another reason for using nanowires instead of bulk material for solar cells is that it has been seen that InP nanowire solar cells can give higher open circuit voltage than their planar equivalent. Possible partly due to different crystal structure in the nanowire (wurtzite instead of zinc blende) compared to bulk InP resulting in larger band gap and that the nanowires have higher absorption per cross-sectional area than planar cells due to having a size comparable to the wave length of the photons [5].

Furthermore a wider variety of materials can be used in heterostructures in nanowire without misfit dislocations than in bulk material due to a smaller interface area[16].

1.3.7 Tandem solar cells

As previously stated (Sec. 1.3.5) all photons with an energy lower than the band gap pass through without being absorbed (giving no current), and all photon energy higher than the band gap becomes heat and is wasted. If there were two layers, a top layer of high band gap material and a bottom layer of lower band gap material (Fig. 9), then more of the energy of the high energy photons would be used, thus more energy from the solar cell. This is the idea behind a tandem solar cell. The efficiency of a tandem solar cell can be optimized if all the high energy photons are absorbed in the top layer and only the low-energy photons reach the bottom layer. The optimal efficiency is 42% with a top layer with band gap 1.9 eV and a bottom layer with a band gap of 1.0 eV. The concept of a tandem cell can be expanded with more layers of a varying band gap, and

indeed the maximum efficiency is 49% with 3 cells up to a maximum of 68% with infinite number of cells. [17]

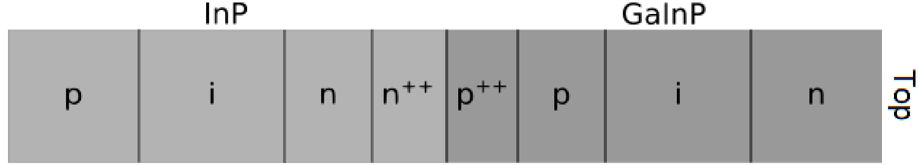

Figure 9: Schematic of a tandem solar cell with illumination from the top. The n^{++} and p^{++} indicate very high doping.

A cell must be connected to a circuit to generate power, but connecting all cells individually is difficult and the connections are possibly decreasing the efficiency of the tandem solar cell. However another possibility is to connect the cells in series but this necessitate a low resistance connection between the cells. If two pn-junctions are connected the interface will create a np-junction, which is just a pn-junction from the other direction. Thus a hill in the potential landscape of the electrons is created and therefore it is not a low resistance connection. However, if there is an Esaki diode between the cells the electrons can tunnel through and a low resistance connection can be achieved [18]. In Fig. 10, an electron-hole pair is first created on the p-side of Cell #1 pn-junction. The electrons drift towards the n-side of Cell #1 due to the electric field and tunnels over the Esaki diode to the valence band of the pn-junction of Cell #2. After the tunneling process, another photon excites the electron to the conduction band of the pn-junction of Cell #2, and the electron is finally collected by an electrical contact on other side of the structure.

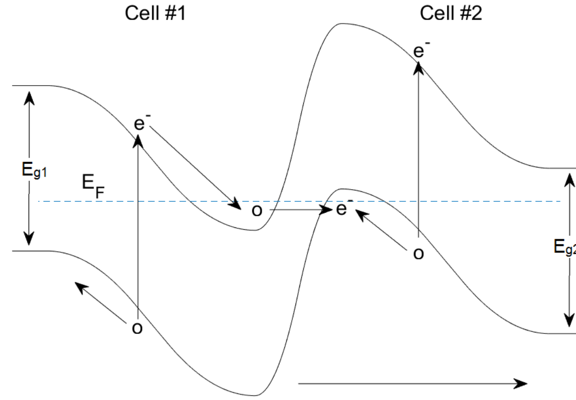

Figure 10: Schematic band structure of a simple tandem solar cell with two pn-junctions connected with an Esaki diode.

1.3.8 npin-structures with an Esaki diode

For some materials the contacts to the p-region have higher resistance, and n-contacts generally have lower resistance. The Esaki diode can then be used as a way of replacing the p-contact by

a combination of a low-resistance n-contact and an Esaki diode, as has been done e.g. for Nitride materials in Ref. [19]. We also study this possibility for InP/GaInP nanowires by simulations in this thesis.

2 Theory and Methods

2.1 WKB-approximation

As mentioned in the introduction the WKB-approximations will be used to create a model for the tunneling current simulations. Here the derivation of the WKB-approximation is presented with its approximations.

The WKB approximation is named after Gregor Wentzel, Hans Kramers and Lon Brillouin who used it to approximately solve the time independent Schrödinger equation in one dimension. The idea behind is to rewrite the time independent Schrödinger equation [20]

$$-\frac{\hbar^2}{2m}\frac{d^2\psi}{dx^2} + V(x)\psi = E\psi \tag{5}$$

as

$$\frac{d^2\psi}{dx^2} = -\frac{p(x)^2}{\hbar^2}\psi \tag{6}$$

where

$$p(x) \equiv \sqrt{2m(E - V(x))} \tag{7}$$

and write the wave function ψ as

$$\psi(x) = A(x)e^{i\phi(x)} \tag{8}$$

Substitute Eq. (8) into Eq. (6), gives

$$\frac{d^2A}{dx^2} + 2i\frac{dA}{dx}\frac{d\phi}{dx} + iA\frac{d^2\phi}{dx^2} - A\left(\frac{d\phi}{dx}\right)^2 = -\frac{p^2}{\hbar^2}A \tag{9}$$

and since there are no imaginary terms on the right side of Eq. (9) they can be set equal to zero and be solved by using the chain rule

$$2\frac{dA}{dx}\frac{d\phi}{dx} + A\frac{d^2\phi}{dx^2} = 0 \Rightarrow \frac{d}{dx}\left(A^2\frac{d\phi}{dx}\right) = 0 \tag{10}$$

and then integrating both sides gives

$$A^2\frac{d\phi}{dx} = C^2 \Rightarrow A = \frac{C}{\sqrt{d\phi/dx}} \tag{11}$$

The real part of Eq. (9) becomes

$$\frac{\frac{d^2A}{dx^2}}{A} = \left(\frac{d\phi}{dx}\right)^2 - \left(\frac{p}{\hbar}\right)^2 \tag{12}$$

and this however cannot be solved analytically. If A is assumed to vary slowly so the left hand side of Eq. 12 is small (≈ 0 compared to $(\phi')^2$ and $p^2/\hbar^2$) then Eq. (12) can be approximated as

$$\frac{d\phi}{dx} = \pm\frac{p}{\hbar} \Rightarrow \phi(x) = \pm\frac{1}{\hbar}\int p(x)dx \tag{13}$$

The wave function is thus a linear combination of the two solutions

$$\psi(x) \approx \frac{C_1}{\sqrt{p(x)}}\exp\left(\frac{i}{\hbar}\int p(x)dx\right) + \frac{C_2}{\sqrt{p(x)}}\exp\left(-\frac{i}{\hbar}\int p(x)dx\right) \tag{14}$$

The transmission probability for a wave of the general form Ae^{ikx} is the outgoing intensity (A_o) divided with the incoming intensity (A_i)

$$T = \frac{|A_o|^2}{|A_i|^2} \tag{15}$$

For the tunneling case ($E < V$) then $p(x)$ is purely imaginary so the exponents are real. This results in one term increasing exponentially and the other decreasing exponentially. But if the tunnel probability is low, and thus the exponentially increasing coefficient is small, it can be neglected. The ratio of the outgoing and incoming amplitudes are then approximated to

$$\frac{|A_o|}{|A_i|} \approx \exp\left(-\frac{1}{\hbar}\int_0^a |p(x)|dx\right) \tag{16}$$

where the barrier starts at $x = 0$ and ends at $x = a$. The absolute value of $p(x)$ replaced the i since $p(x)$ is imaginary. This gives the tunnel probability

$$T = \frac{|A_o|^2}{|A_i|^2} \approx \exp\left(-\frac{2}{\hbar}\int_0^a |p(x)|dx\right) \tag{17}$$

Using the approximated band diagram from Fig. 11 the electrons always have the same tunnel distance and barrier height regardless of the electrons energy. Therefore $p(x)$ can be written as [8]

$$p(x) = \sqrt{2m(-q\mathscr{E}x)} \tag{18}$$

since $-q\mathscr{E}$, where $\mathscr{E}$ is the electric field, is the slope of the conduction band. This also results in the tunneling distance (upper limit of the integral in Eq. (17)) $a = E_g/q\mathscr{E}$. Using this and solving the integral in the exponential gives

$$T = \exp\left(-\frac{4\sqrt{2m}E_g^{3/2}}{3q\hbar\mathscr{E}}\right) \tag{19}$$

for tunneling in one dimension where E_g is the band gap. If the electrons have energy in the y and z directions as well an additional term need to be added. The electron goes diagonally through the barrier instead of straight as in one dimension and thus has a longer tunneling distance and lower tunneling probability. If the perpendicular energy ($E_\perp$) is considered the tunneling probability then becomes [21]

$$T = \frac{\pi^2}{9}\exp\left(-\frac{2E_\perp}{\bar{E}}\right)\exp\left(-\frac{4\sqrt{2m}E_g^{3/2}}{3q\hbar\mathscr{E}}\right) \tag{20}$$

where

$$E = E_x + E_\perp \tag{21}$$

and

$$\bar{E} = \frac{\sqrt{2} q \hbar \mathscr{E}}{\pi \sqrt{m^* E_g}} \tag{22}$$

The tunnel current is an integration of the product of the Fermi function($F_{C(V)}(E)$), the density of states ($N_{c(v)}(E)$), the tunneling probability (T), the probability for empty states on the other side ($1 - F_{V(C)}(E)$) and the density of states on the other side ($N_{v(c)}(E)$). The total current then becomes

$$I = I_{C\to V} - I_{V\to C} = C \int_{E_{Vp}}^{E_{Cn}} [F_C(E) - F_V(E)] T N_c(E) N_v(E) dE \tag{23}$$

where C is a constant. Writing this equation with the help of Eq. (20), Sze and Kwok propose a form that has also been used in simulations throughout this thesis [8]

$$J_t = \frac{q^2 \mathscr{E}}{36\pi\hbar^2} \sqrt{\frac{2m^*}{E_g}} \exp\left(-\frac{4\sqrt{2m^*} E_g^{3/2}}{3q\hbar\mathscr{E}}\right) D \tag{24}$$

where D is defined as

$$D \equiv \int (F_C(E) - F_V(E)) \left[1 - \exp\left(-\frac{2E_S}{\bar{E}}\right)\right] dE \tag{25}$$

where F_C and F_V is the Fermi function from the conduction band and valence band respectively and E_S is the smallest of E_1 and E_2 (see Fig. 11). The average electric field can be expressed as

$$\mathscr{E} = \sqrt{\frac{q(\Psi_{bi} - V) N_A N_D}{2\epsilon_s (N_A + N_D)}} \tag{26}$$

where Ψ_{bi} is the built-in potential and $N_{A(D)}$ is the acceptor (donor) concentration. The effective tunneling mass used in Eq. (24) is

$$m^* = 2\left(\frac{1}{m_e^*} + \frac{1}{m_{lh}^*}\right) \tag{27}$$

where m_e and m_{lh} are the effective electron mass and the effective light-hole mass respectively. In a heterostructure the effective band gap is given by [22]

$$E_g = E_g^{p-side} - \Delta E_c \tag{28}$$

where ΔE_c is estimated as the difference in electron affinities.

Because of the uncertainties in the model the peak current will be scaled to measured peak current. The effect of changing doping will be investigated under the assumption that the current difference between model and experimental data is only due to a prefactor independent of doping.

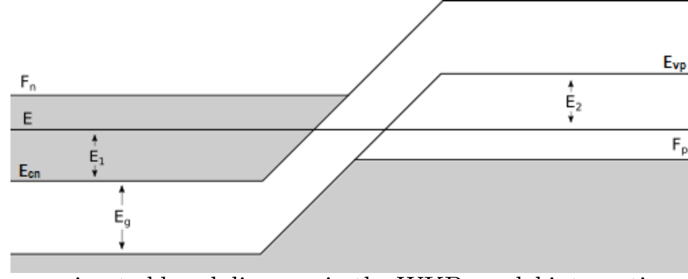

Figure 11: Approximated band diagram in the WKB-model integrating over E between E_{cn} and E_{vp}, E_1 and E_2 as the distance from the conduction band and valence band respectively to E. $F_{n(p)}$ is the quasi fermi level on the n(p)-side

2.2 Drift-Diffusion model

Drift-diffusion model is the standard choice to simulate full devices such as npin structures and to explain current transport processes in pn junctions and solar cells. The tunnel junction model is also integrated with drift-diffusion simulations in this thesis. Therefore we summarize the drift-diffusion model here.

Drift-Diffusion model is an approximation derived from the Boltzmann transport equation (BTE)

$$\frac{df}{dt} = \left(\frac{\partial f}{\partial t}\right)_{scatt} \tag{29}$$

where $f(\vec{r}, \vec{k}, t)$ is the probability distribution function and the right side term is the scattering. So without scattering f is not changing in time. After expanding the left hand side of Eq. (29) using the chain rule and some well-known physical definitions it can be rewritten in the following way [23]

$$\frac{\partial f}{\partial t} + \frac{\vec{F}_{ext}}{\hbar} \cdot \vec{\nabla}_k f + \vec{v} \cdot \vec{\nabla}_x f = \left(\frac{\partial f}{\partial t}\right)_{scatt} \tag{30}$$

where $\nabla_{r(k)}$ is the nabla operator with respect to $\vec{r}$ ($\vec{k}$), $\vec{v}$ is the velocity and $\vec{F_{ext}}$ are the external forces. Notable here is that the probability function is defined as a function of $\vec{r}$ and $\vec{k}$ and Heisenberg's uncertainty principle state that both $\vec{r}$ and $\vec{k}$ cannot be know at the same time and BTE is thus valid only in the classical limit. Further for the drift-diffusion model, the scattering is approximated as

$$\left(\frac{\partial f}{\partial t}\right)_{scatt} = -\frac{f - f_0}{\tau} \tag{31}$$

where f_0 is the distribution function at equilibrium and τ is the relaxation time of the system that determines how fast it returns to equilibrium after a perturbation. Thus the further away from equilibrium the system is the more scattering occurs to bring it back to equilibrium.

When Eq. (31) is used in Eq. (30) and the equation is multiplied by $\vec{v}$ and integrated over $\vec{k}$ Eq. (30) becomes

$$\int \vec{v}\frac{\partial f}{\partial t} d^3k + \frac{1}{\hbar}\int \vec{v}(\vec{F}_{ext} \cdot \vec{\nabla}_k f) d^3k + \int \vec{v}(\vec{v} \cdot \vec{\nabla}_x f) d^3k = -\int \vec{v}\frac{f - f_0}{\tau} d^3k \tag{32}$$

To derive the drift-diffusion model a parabolic band structure, an isotropic mass and no temperature gradient are assumed. Furthermore, a zero-order approximation is used neglecting the derivatives of t and assuming quasi-equilibrium distributions. After substitutions are made the drift-diffusion equations are reached for electrons (Eq. (33)) and holes (Eq. (34)) [23]

$$J_n = qn\mu_n\vec{\mathscr{E}} + qD_n\vec{\nabla}_r n \tag{33}$$

$$J_p = qp\mu_p\vec{\mathscr{E}} - qD_p\vec{\nabla}_r n \tag{34}$$

where $n(p)$ is the electron (hole) concentration, $\mu_{n(p)}$ is the electron (hole) mobility and $D_{n(p)}$ is the diffusion constant for electrons (holes). The full drift-diffusion model is obtained by complementing Eqs. (33) and (34) with the Poisson equation for self-consistent electrostatic field, and the model can be implemented for example using the finite-element method. Finally, the band edges and quasi-Fermi levels can be used to integrate the tunneling current of Eq. (24) with the drift-diffusion model.

2.3 Current transport in pn-junctions

We already discussed the current transport in normal pn junctions phenomenologically in the introduction (Sec. 1.3.3). Here we describe a more detailed form for the current based on the theoretical models presented in the previous subsections. As mentioned in Sec. 1.3.3 there are two mechanisms, drift and diffusion, that dominate the transport in a pn-junction. Drift is due to an electric field, either external or caused by e.g. a pn-junction, that shift the movement of the electrons from random in every direction with a net velocity of zero to random movement with a bias in the direction of the electric field. This cause a net velocity in the direction of the electric field and thus current.

Diffusion is random movements of e.g. electrons, and diffusion current occurs when there is a concentration (or temperature) gradient. If at a point there are more electrons on one side than on the other side, and the electrons are moving in all directions, there will be more electrons coming from the side with more electrons than from the side with less electrons and thus there will be a electron transport. Similarly if there is a temperature gradient the electrons will move faster on one side than the other, and thus there will be more electrons moving from high temperature than thus electrons will have a net movement from high temperature to low temperature. [6]

In a pn-junction there are simultaneously drift and diffusion transport. There is drift transport of electrons from the p-side to the n-side due to the electric field in the depletion region created by the ionized dopant atoms. There is also diffusion transport from the n-side to the p-side due to higher concentration of electrons on the n-side. The drift current is determined by the amount of electrons on the p-side close to the junction.

The diffusion current depends on how many electrons there are close to the junction with enough energy in the direction of the junction. The number of electrons is described by the Fermi function (Eq. (1) see also Fig. 2) which is an exponentially decaying function with energy, so it is exponentially dependant on the barrier height of the pn-junction. Forward bias is decreasing the barrier height and reverse bias is increasing the barrier height.

So with reverse bias the drift current is almost unchanged, but the diffusion current goes towards zero, thus reaching an almost constant current for reverse bias. With forward bias the drift current is almost constant but the diffusion current is exponentially increasing with bias. This motivates the Ideal diode equation[24]

$$I = I_0\left[\exp\left(\frac{qV}{\eta k_B T}\right) - 1\right] \tag{35}$$

where V is the bias and η is the ideality factor which is one for an ideal diode but for real diodes typically range between one and two. In non-degenerate semiconductors I_0 is given by

$$I_0 = qA \left(\sqrt{\frac{D_p}{\tau_p}} \frac{n_i^2}{N_D} + \sqrt{\frac{D_n}{\tau_n}} \frac{n_i^2}{N_A} \right) \tag{36}$$

where A is the cross section area, $D_{n(p)}$ is the diffusion constant for electrons (holes), $\tau_{n(p)}$ is the electron (hole) minority carrier lifetime and n_i is the intrinsic carrier concentration of the semiconductor.

2.4 Band tailing

The band structure is characteristic for a specific material and adding dopants will change the material slightly and therefore also the band structure. Dopants in a semiconductor create energy levels for electrons inside the band gap [25] (see Fig. 12). As the doping density gets higher the energy states start to merge with each other to form a band that connects to the conduction or valence band extending the band. This makes the band gap smaller and since the dopants are not uniformly distributed and some parts will have a higher dopant density and other parts a lower dopant density the band extension also change the shape of the bottom (top) of the conduction (valence) band as seen in Fig. 13 [26]. Changes in band gap change the voltage range for which there can be tunneling current and potentially also the peak current voltage (see Fig. 11). The band structure is also changed and this can affect the current, which depends on the band gap and the dispersion relation of the degenerately doped material.

The band narrowing has been shown to be described well by [27]

$$\Delta E_g = AN^{1/3} + BN^{1/4} + CN^{1/2} \tag{37}$$

where A, B and C are material specific constants and N is the doping.

2.5 Uncertainties in the tunneling model

There are many approximations going into the simulations that are done in this thesis. The triangular potential barrier is shown (in Sec. 3.1) not to be appropriate for higher doping. The abrupt junction approximation is also a crude approximation as for example Wheeldon *et al.* in Ref. [28] modifies the doping level with a factor 0.73 to get the active dopant concentration in AlGaAs Esaki diodes. This factor takes into account diffusion of the dopant atoms between the sides of the pn-junction.

In addition, the band tailing effect discussed in the previous subsection is not accounted for in the model derived in Sec. 2.1, and it presumably affects at least the peak voltage in the measurements. Due to these uncertainties we also compare the IV characteristics from simulations with available experimental data and discuss the possible reasons for the differences between the WKB calculations and measurements. Finally we give suggestions on how to develop more sophisticated and accurate models in subsequent works.

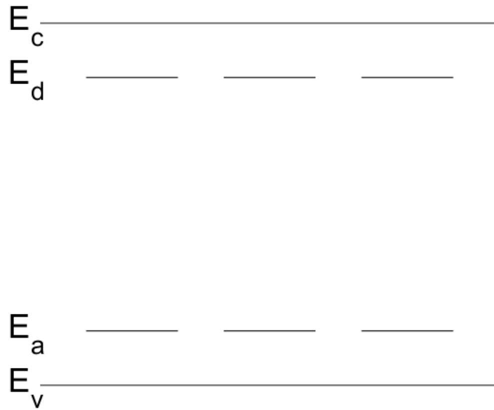

Figure 12: Band diagram of a doped semiconductor with energy states in the band gap from donors (E_d) and acceptors (E_a).

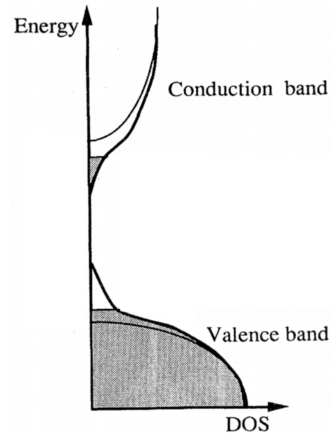

Figure 13: Schematic change in band structure as the result of band tailing. Thin line is for undoped semiconductor and thick line is for heavily doped semiconductor. Adapted from Ref. [26]

2.6 Nanowire growth

Growth of nanowires are outside the scope of this thesis, however measured data has been received from nanowires grown by metalorgranic vapor-phase epitaxy (MOVPE). An overview will be given of the growth process.

Vapor-phase epitaxy is a method for growing a semiconductor one atom layer at the time onto the substrate. This is done by adding vapor of compounds (precursors) that react with each other and add a layer of the wanted material to the substrate [29]. The substrate is heated up so that the reaction will take place at the surface of the substrate. If metalorganic precursors are used it is MOVPE. E.g. the compounds used to grow InP in the nanowires examined in this thesis were trimethylindium (TMI) and phosphine (PH_3) which simplified can be described by reaction [30]

$$\mathrm{In(CH_3)_3 + PH_3 \rightarrow InP + 3CH_4} \tag{38}$$

More precursors can be added to dope the material or to fabricate ternary or quaternary alloy.

When nanowires are grown with MOVPE the growth needs to be limited to the nanowires and not the surrounding substrate. The most common method to limit the growth and the method used for the nanowires measured in this thesis is to use an Au seed particle [31]. The temperature is lower than required for film growth so the seed particle is needed catalyse the growth and thus the nanowire grows under the seed particle. Since the seed particle catalyse the growth the size of the seed particle determine the size of the nanowire, and how long time the precursors are in the growth chamber determine the length of the nanowire. The size of the nanowires measured for this thesis is a diameter of around 180 nm and a length of around 2 μm. The nanowires have acceptor (donor) doping levels of 2×10^{18} (10^{19}).

3 Results and Discussion

Here we present the samples, simulations, and analyses of experimental data. In Sec. 3.1 simulations are presented, first of the IV-characteristics simulated for the same doping levels as the experimental data and then for different dopings. In Sec. 3.2 the data obtained from the measurements is presented and discussed. Sec. 3.3 simulations are presented of how the simulated tunneling current would be affected by contact resistance. The exponential diode current law with a series resistance is fitted in Sec. 3.4 for two nanowires to estimate the ideality factor and contact resistance and in Sec. 3.5 the Esaki simulations are imported to a comsol model to simulate the IV characteristics for a npin-sturcture.

All experimental data and simulations are for InP/$Ga_{0.25}In_{0.75}P$ nanowire with a diameter of 180 nm, a InP n-doping of 10^{19} cm^{-3} and a GaInP p-doping of 2×10^{18} cm^{-3} unless otherwise stated.

3.1 Current simulated with WKB-approximation

The IV-simulation of the tunnel current by the WKB-approximation (Eq. (24)) is presented in Fig. 14. The current is calculated by integrating over the tunneling energy range starting from the n-side conduction band edge to the p-side valence band edge (Fig. 11). The large increase in current for low applied bias is due to the increasing density of states further from the band edges.

As the bias is increased the tunneling energy gap becomes smaller, and less states are available for tunneling. Close to the band edges there are a lower density of states and therefore as the integrated energy range decreases (by applying forward bias) the current is decreasing less per unit bias (see Fig. 6).

As seen in the figure there is no current after about 0.15 V, and this corresponds to the difference in energy of the n-side conduction band and the p-side valence band under zero applied bias. In the simulations only direct tunneling is considered and thus electrons must retain their energy when going through the barrier, and there must be a filled state to tunnel from and an empty state to tunnel to. At an applied bias of 0.15 V the band edges are aligned, and therefore no direct tunneling is possible any more.

In Fig. 15 and 16 the peak current and peak current voltage respectively are plotted for different acceptor doping densities as a function of the donor density. The current density has been scaled with a constant factor obtained from one sample to reproduce the peak current from the measurements, and the same scaling factor has been used in all the other devices simulated in Fig. 15, since we only change the doping levels in the simulations whose effects on the current are already accounted for through Eq. (24). Larger doping densities decrease the tunneling distance and increase the number of states available for tunneling (increases the difference between n-side conduction band edge and the p-side valence band edge, see Fig.6), and it can also be seen in Fig. 15 that the peak current increases strongly with both acceptor and donor doping. Naturally there is no current for low doping levels since tunneling is not possible, but as seen in the Fig. 15 low doping on one side can be compensated with higher doping on the other side.

In Fig. 16 the peak current voltages are increased as the doping increases. The peak current voltage increases due to the increase in built-in potential as the doping increases. This creates a larger window for tunneling and since the densities of states increase further away from the band edge this also shifts the tunnel current voltage.

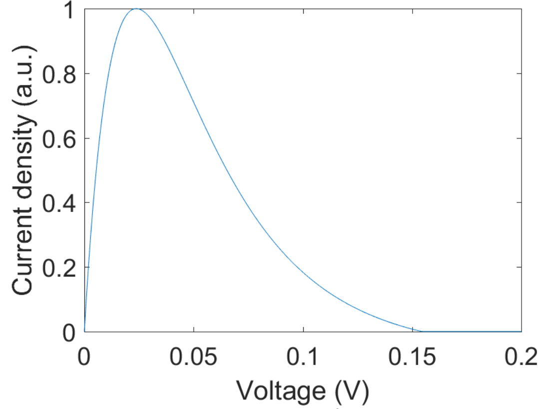

Figure 14: Simulated IV characteristic of the tunnel current by the WKB-approximation of the InP/GaInP nanowire Esaki diode.

Note that the simulations yield an unreasonably high current for high doping as the simulated current per nanowire reaches 10^{16} A with both N_a and N_d at 5×10^{19} cm^{-3}, compared to the value of 0.8 nA also included in the figure for the device with N_a=2×10^{18} cm^{-3} and N_d=10^{19} cm^{-3} for which there is experimental data. The electric field increases with the doping directly in Eq. (26) but also indirectly since increase doping increases the built-in potential. In Eq. (24) the electric field both linearly and exponentially increases the prefactor of the tunneling current. Not as obvious is that as the n-doping increases, the Fermi level also increases compared to the conduction band on the n-side, resulting in more states being filled. As the p-doping increases the fermi level decreases and thus more states are empty on the p-side (see Fig. 17). Both these affect the tunneling current exponentially (see Eq. (1) and (23)), increasing the current from the n-side to the p-side.

The unreasonable current for high doping can be explained with the help of comsol simulations of the band diagrams simulated for Esaki diodes at zero bias shown in Fig, 17. Comparing the predictions of the band diagram approximation with these band diagrams shows that the band diagram approximation underestimates the tunneling distance for high doping and therefore overestimate the tunneling current. For the doping of the experimental data comsol simulation gives a tunneling distance of $\approx$ 29.5 nm (Fig. 17(a)) and the band diagram approximation gives 30.8 nm. However for doping levels of 5×10^{19} on both sides the comsol simulation gives a tunneling distance of $\approx$ 8.8 nm (Fig. 17(b)) and the band diagram approximation gives 6.9 nm, a result that is 21% lower than comsol simulations. This yields a large overestimation of the tunneling current since the current it decreasing exponentially with tunnel distance. However this effect is not sufficient to explain the discrepancy since it changes the current with a factor 10^5. Furthermore the approximation also assumes an abrupt junction for the doping which is not possible to fabricate, and the deviation from the ideal abrupt junction can be expected to increase strongly with doping.

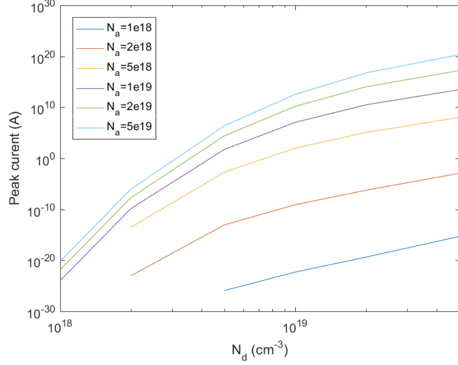

Figure 15: Peak current as a function of donor doping for different levels of acceptor doping. The current is scaled with a factor to fit the current from the experimental data point where N_a=2 × 10^{18} cm^{-3} and N_d=10^{19} cm^{-3}.

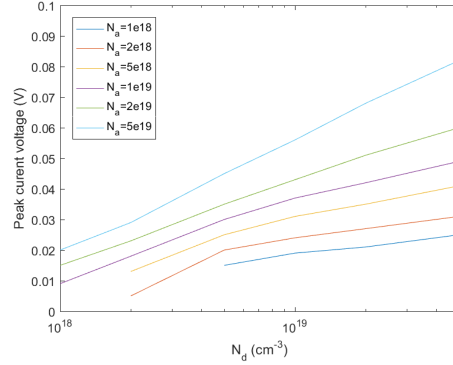

Figure 16: Peak voltage as a function of donor doping for different levels of acceptor doping.

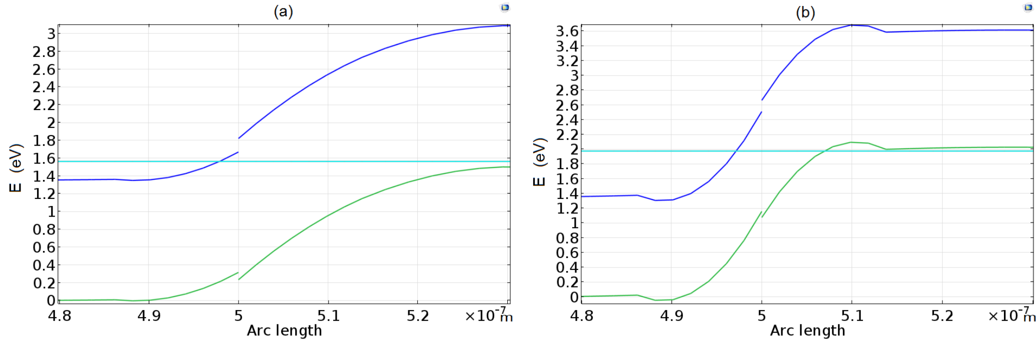

Figure 17: Band diagram of a InP-$Ga_{0.25}In_{0.75}P$ heterojunction in equilibrium. The discontinuity is due to the difference in band gap for the different materials. In (a) the doping levels are 2×10^{18} (10^{19}) for the p-side (n-side) and the tunneling distance is $\approx$ 29.5 nm. In (b) both doping levels are 5×10^{19} and the tunneling distance is $\approx$ 8.8 nm. All band parameters for the comsol simulations are from Ref. [32]

3.2 Measured tunneling IV characteristics

In the previous subsection we used in-house measurements of a nanowire Esaki diode to scale the peak current given by the WKB-approximation. In this subsection we compare the predictions from the WKB-approximations with experiments in more detail. The empirical data in this report are measurements from five nanowires from one sample grown with MOVPE. Their IV-characteristics is presented in Fig. 18. As seen from the figure there is one nanowire (NW #3) that does not show Esaki diode IV-characteristic and has hence been disregarded. This is probably due to too low active doping level that may be due to diffusion between the n- and p-sides. The other four show roughly similar IV-characteristic.

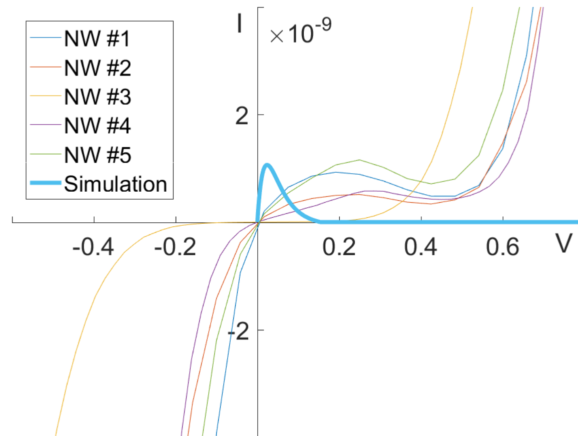

Figure 18: Measured data from five different nanowires from one sample grown with MOVPE shown together with the simulated tunneling current from Fig. 14. The X-axis is the total voltage.

The peak value of the current is expected to be different between the simulations and experiments due to band (triangular barrier and neglecting band tailing) and abrupt junction approximations and thus we already fitted in the previous subsection the peak current from the simulations with the measured peak current (see Sec. 2.5). There is however, also a large difference in the voltage corresponding to the peak current (referred to from now on as peak current voltage) between the simulated voltage of 25 mV and the measured nanowires with peak current voltage of 190-290 mV. This peak current voltage is also higher than the maximum voltage of about 150 mV which allowed tunneling current in the simulation because it corresponds to when the n-side conduction band edge and p-side valence band edge have the same energy. According to the model no tunnel current can flow with higher applied bias. Possible explanations for this are discussed in the next section.

3.3 Tunneling current with contact resistance and band tailing

The simulated voltage is the voltage drop over the diode whereas the measured voltage (V) includes the voltage drop over the contacts due to contact resistances. In Fig. 19 simulation has been done for NW #1 and NW #4 to simulate the effect of added contact resistance. NW #1 and #4 was chosen because they have the most different peak voltage. This will show the difference between nanowires within one sample. A fitting of contact resistance (R_c) has been done for these nanowires so that the peak current of the simulations are at the peak current of the measured data by replacing V_{diode} with $V = V_{diode} + IR_c$ (as in Ref. [22],[28]). Figure 19 shows the fit with matching peak current voltage for NW #1 and NW #4. The presence of a contact resistance cannot alone explain the shape and the position of the peak current (For more plots of different resistances see Appendix A). An artefact from the simulations is when the current through the Esaki diode decreases in the negative differential resistance region, the voltage drop over the contacts also decreases, resulting in a decreasing total voltage. Similar artefact has been observed elsewhere in a simulation of a similar system including an Esaki diode and a series resistance [28].

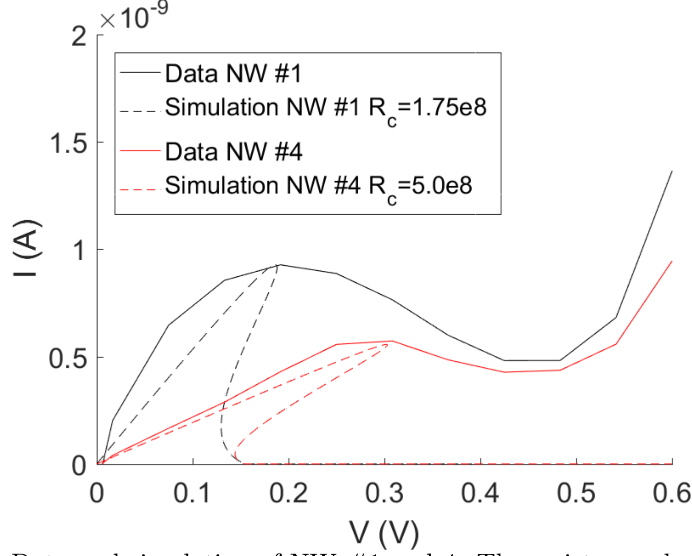

Figure 19: Data and simulation of NW #1 and 4. The resistance shown is chosen so that the peak currents of the data and simulations are similar.

Band tailing is another possible contributor to the peak current voltage increase since it lower the conduction band edge on the n-side and raise the valence band edge on the p-side it creates a wider energy range for tunneling (see Fig. 6). The increased energy range is about 0.4 eV for InP at present doping levels used in the present experimental sample (Eq. (37))[1] which is about the voltage range for the tunnel current in the measurements (Fig. 18). Since band tailing is not considered in the simulations and the increased tunneling energy range is significant this may explain the underestimated peak current voltage of the simulations as compared to the experimental IV curves.

3.4 Measured diode IV characteristics

In this subsection we study the diode currents of the samples at voltages above the direct tunneling regime. In Fig. 20 we plot the measured IV curves and fit the ideality factor (η) and I_0 of Eq. (35) and a series resistance (R_c) to the experimental curves.

In Fig. 20 IV characteristics of NW #1 and #4 are shown together with the IV curves fitted to the data using Eq. (35) and a series resistance. The simulations for the contact resistance starts from 0.4 V for it to be after the tunnel peak so that only the excess current contribute. The minus one part of Eq. (35) is omitted for the fitting since the exponential term is much larger than one. As seen, the resistances here are two to four orders of magnitude different from the contact resistances

[1] A, B and C are 1.72×10^{-8} eV·cm, 2.62×10^{-7} eV·cm$^{3/4}$ and 9.84×10^{-11} eV·cm$^{3/2}$ respectively for the n-side and 1.03×10^{-8} eV·cm, 4.43×10^{-7} eV·cm$^{3/4}$ and 3.38×10^{-12} eV·cm$^{3/2}$ [27] respectively for the p-side.

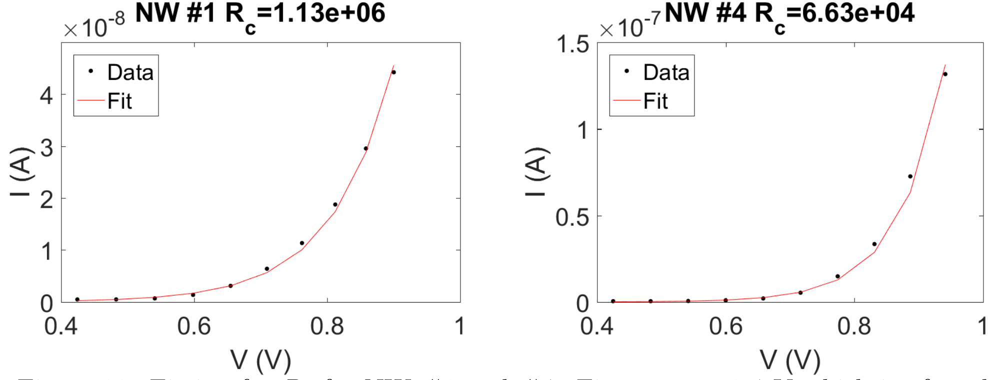

Figure 20: Fitting for R_c for NW #1 and #4. Fit starts at 0.4 V which is after the tunnel peak.

generating the correct peak current voltage (Fig. 19). This also indicates that other explanations than contact resistance are required to explain the shape of the peak current and value of the peak current voltage.

From the fitting of the curves the factor in the exponent is obtained with which an ideality factor (η)(see Eq.(35)) can be calculated to 3.5 and 2.7 for NW #1 and #4 respectively. The normal value of the ideality factor is 1-2 (1 for diffusion current, 2 for recombination current and between when there is a mix of the different currents). It has however been shown that ideality factors over 2 can occur due to trap assisted tunneling [33] which means that there are states in the band gap that the electrons can tunnel to and then recombine with the holes in the valence band.

3.5 Simulation of npin-structure

Finally we apply the model to a npin-structure by integrating the IV data from the Esaki diode with the drift diffusion model, in this subsection we show initial simulations of an npin-structure, where the pin-structure is simulated with the full drift-diffusion model and the np-Esaki diode is realized with the Esaki diode IV data.

In Fig. 21 the current density is plotted versus bias voltage for a npin with Esaki diode data from the WKB-simulations and for a pin without an Esaki diode. There is a difference in voltage for the two structures due to a voltage drop over the Esaki diode. This increases the voltage over the whole structure as compared with the pin-structure without the Esaki diode. Note, however, that both structures are simulated here without accounting for contact resistance.

Electron-hole generation is added as a constant rate in the comsol simulations in the intrinsic region for the IV-characteristics shown in Fig. 22. The generation of electrons and holes simulates the excitation of electrons and holes due to photons. As can be seen in the figure there is a current for zero bias since the electrons generated drift due to the built-in electric field. This results in a small offset between the illuminated and the dark current. In the illuminated case in Fig. 22 electrons first tunnel from n- to p-side through the Esaki diode and flow to the i-region where they are excited to the conduction band, after which they transport to the n-contact of the pin-junction.

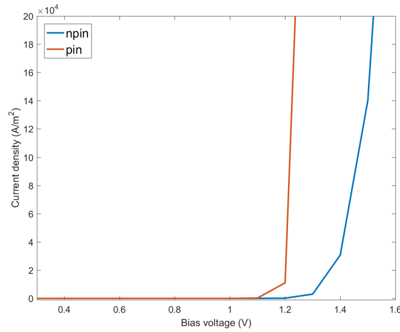

Figure 21: Simulation of current density verses bias voltage for a pin- and a npin-structure with an Esaki diode. The voltage drop over the esaki diode delays the exponential current increase fron the pin-junction.

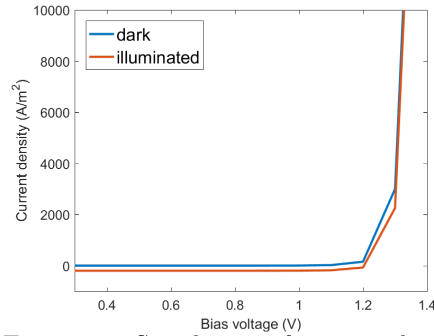

Figure 22: Simulation of current density verses bias voltage for a npin-structure with an Esaki diode with and without and electron generation in the intrinsic region. The generation creates a current even for no applied bias.

4 Conclusions

To create nanowire-based multi-junction solar cells, better understanding is needed on nanowire Esaki diodes. In this thesis, a simulation model was developed based on the WKB-approximation and the results were compared to available experimental data.

The current calculations with the WKB-approximation lead to a surprisingly strong dependence of the peak tunneling current on the doping densities. A more realistic current was expected, this is most probably due to approximations used in the simulation model especially for the exact form of the tunnel barrier. Based on the simulations, systematic experimental studies are suggested to enable comparing the simulated dependence of doping density with experiments.

We conclude that better methods need to be utilized for simulation of tunnel current with i.e. band tailing or quantum transport models (with i.e. NEMO5) using a full-band description. For use in drift-diffusion simulations empirical data from Esaki diodes could also be used to simulate i.e. tandem solar cells as was preliminary done in this thesis in the simulation of a npin-structure including an Esaki diode.

The experiments also showed much larger Esaki diode peak current voltages than what was expected from the band diagrams calculated for the diodes. It was shown in the thesis that contact resistance alone was unable to explain this, and therefore band tailing effects due to high doping were suggested as a possible explanation for the high peak voltages measured and thus is a necessary component in future simulations.

Investigations of the measured excess current, on the other hand, showed that the excess current has an exponential form with ideality factors larger than 2, possibly indicating that the excess current consisted of trap-assisted tunneling.

References

[1] Q. Zhang, J. Chang, T. Wang, and Y. Xu, "Review of biomass pyrolysis oil properties and upgrading research," *Energy Conversion and Management*, vol. 48, pp. 87–92, 2007.

[2] J. S. Cha, S. H. Park, S.-C. Jung, C. Rye, J.-K. Jeon, M.-C. Shin, and Y.-K. Park, "Production and utilization of biochar: A review," *Journal of Industrial and Engineering Chemistry*, vol. 40, pp. 1–15, 2016.

[3] T. Ameri, G. Dennler, C. Lungenschmied, and C. J. Brabec, "Organic tandem solar cells: A review," *Energy 6 Environmental Science*, vol. 2, pp. 347–363, 2009.

[4] International Energy Agency, "Key world energy statistics." www.iea.org, 2016.

[5] J. Wallentin, N. Anttu, D. Asoli, M. Huffman, I. Åberg, M. H. Magnusson, G. Siefer, P. Fuss-Kailuweit, F. Dimroth, B. Witzigmann, H. Q. Xu, L. Samuelson, K. Deppert, and M. T. Borgstrm, "Inp nanowire array solar cells achieving 13.8% efficiency by exceeding the ray optics limit," *Science*, vol. 339, no. 6123, pp. 1057–1060, 2013.

[6] G. Grossmann, *Fasta tillståndets fysik*. Lunds Universitet, 2014.

[7] C. T. Jones, *Hybrid High Temperature Superconductor / Conducting Polymer Systems*. PhD thesis, University of Texas, 1990.

[8] S. Sze and K. Kwok, *Physics of Semiconductor Devices, 3rd Edition*. John Wiley and Sons, Inc, 2007.

[9] J. H. Davies, *The physics of low-dimensional semiconductors: an introduction*. Cambridge University Press, 2006.

[10] M. O. Manasreh, *InP and related compounds: materials, applications and devices*. Gordon and Breach Science Publishers, 2000.

[11] B. van Zeghbroeck, *Principles of Semiconductor Devices*. University of Colorado Boulder, 2011.

[12] L. Esaki, "New phenomenon in narrow germanuim p-n junctions," *Physical Review*, vol. 109, no. 2, pp. 603–604, 1957.

[13] B. E. A. Saleh and M. C. Teich, *Fundamentals of Photonics*. Hoboken, N.J., 2007.

[14] W. Shockley and H. J. Queisser, "Detailed balance limit of efficiency of pn junction solar cells," *Journal of Applied Physics*, vol. 32, no. 3, pp. 510–519, 1961.

[15] Y. Chen, M.-E. Pistol, and N. Anttu, "Design for strong absorption in a nanowire array tandem solar cell," *Scientific Reports*, vol. 6, pp. 32349–32357, 2016.

[16] E. Ertekin, P. A. Greaney, D. C. Chrzan, and T. D. Sands, "Equilibrium limits of coherency in strained nanowire heterostructures," *Journal of Applied Physics*, vol. 97, no. 11, 2005.

[17] A. De Vos, "Detailed balance limit of the efficiency of tandem solar cells," *Journal of Physics D, Applied Physics*, vol. 13, no. 5, pp. 839–846, 1980.

[18] B. Sciana, I. Zborowska-Lindert, D. Radziewicz, D. Pucicki, M. Panek, J. Jurenczyk, W. Dawidowski, M. Badura, and M. Tlaczala, "Tunnel junction technology for multijunction solar cell applications," 2012.

[19] E. C. Young, B. P. Yonkee, F. Wu, S. H. Oh, S. P. DenBaars, S. Nakamura, and J. S. Speck, "Hybrid tunnel junction contacts to III-nitride light-emitting diodes," *Applied Physics Express*, vol. 9, no. 2, 2016.

[20] D. J. Griffiths, *Introduction to Quantum Mechanics.* Prentice Hall, Inc., 1995.

[21] E. O. Kane, "Theory of tunneling," *Journal of Applied Physics*, vol. 32, no. 1, pp. 83–91, 1961.

[22] W. Y. Fung, L. Chen, and W. Lu, "Esaki tunnel diodes based on vertical Si-Ge nanowire heterojunctions," *Applied Physics Letter*, vol. 99, no. 9, 2011.

[23] K. F. Brennan, *The Physics of Semiconductors: with application to optoelectronic devices.* Cambridge University Press, 1999.

[24] E. F. Schubert, *Light-Emitting Diodes.* Cambridge University Press, 2006.

[25] H. Ibach and H. Lüth, *Solid-State Physics.* Springer, 2009.

[26] P. V. Mieghem, "Theory of band tails in heavily doped semiconductors," *Review of Modern Physics*, vol. 64, no. 3, pp. 755–793, 1992.

[27] S. Jain, J. M. McGregor, and D. Roulston, "Band-gap narrowing in novel III-V semiconductors," *Journal of Applied Physics*, vol. 68, pp. 3747–3749, 1990.

[28] J. F. Wheeldon, C. E. Valdivia, A. W. Walker, G. Kolhatkar, A. Jaouad, A. Turala, B. Riel, D. Masson, N. Puetz, S. Fafard, R. Ars, V. Aimez, T. J. Hall, and K. Hinzer, "Performance comparison of algaas, gaas and ingap tunnel junctions for concentrated multijunction solar cells," *Progress in Photovoltaics: Research and Applications*, vol. 19, no. 4, pp. 442–452, 2011.

[29] G. S. May and S. M. Sze, *Fundamentals of Semiconductor Fabrication.* John Wiley and Sons, Inc, 2004.

[30] A. Owens, *Compound Semiconductor Radiation Detectors.* CRC Press, 2012.

[31] R. G. Hobbs, N. Petkov, and J. D. Holmes, "Semiconductor nanowire fabrication by bottom-up and top-down paradigms," *Chemistry of materials*, vol. 24, no. 11, pp. 1975–1991, 2012.

[32] I. Vurgaftman, J. R. Meyer, and L. R. Ram-Mohan, "Band parameters for iiiv compound semiconductors and their alloys," *Journal of Applied Physics*, vol. 89, no. 11, pp. 5815–5875, 2001.

[33] M. Mandurrino, G. Verzellesi, M. Goano, M. Vallone, F. Bertazzi, G. Ghione, M. Meneghini, G. Meneghesso, and E. Zanoni, "Physics-based modeling and experimental implications of trap-assisted tunneling in ingan/gan light-emitting diodes," *Physica Status Solidi (a)*, vol. 212, no. 5, pp. 947–953, 2015.

Appendix A Contact resistance sweeps

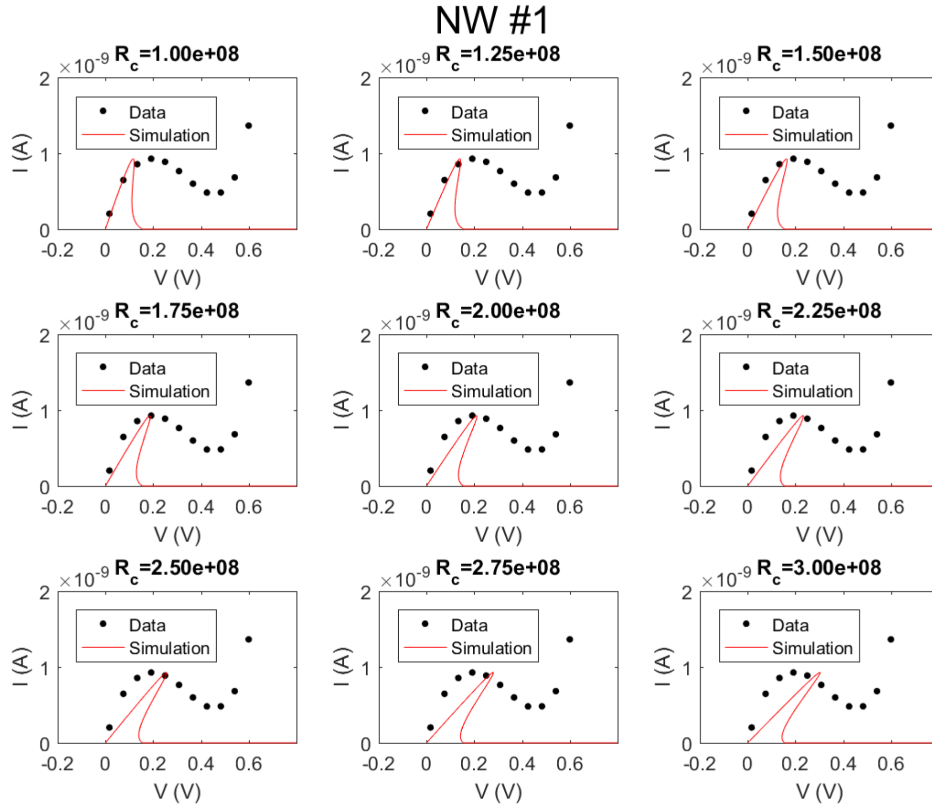

Figure 23: Simulation of the effect of the contact resistance compared to the measured IV-characteristic of NW #1. At $R_c = 1.75 \times 10^8$ the peak current voltage is same as for the data.

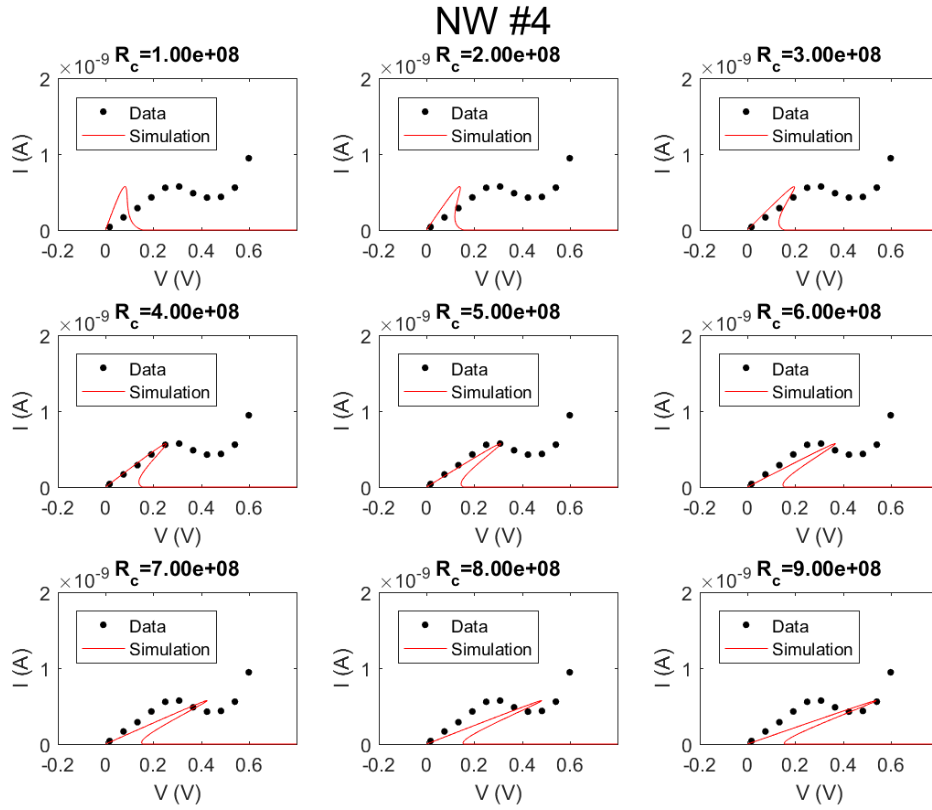

Figure 24: Simulation of the effect of the contact resistance compared to the measured IV-characteristic of NW #4. At $R_c = 5.0 \times 10^8$ the peak current voltage is same as for the data.

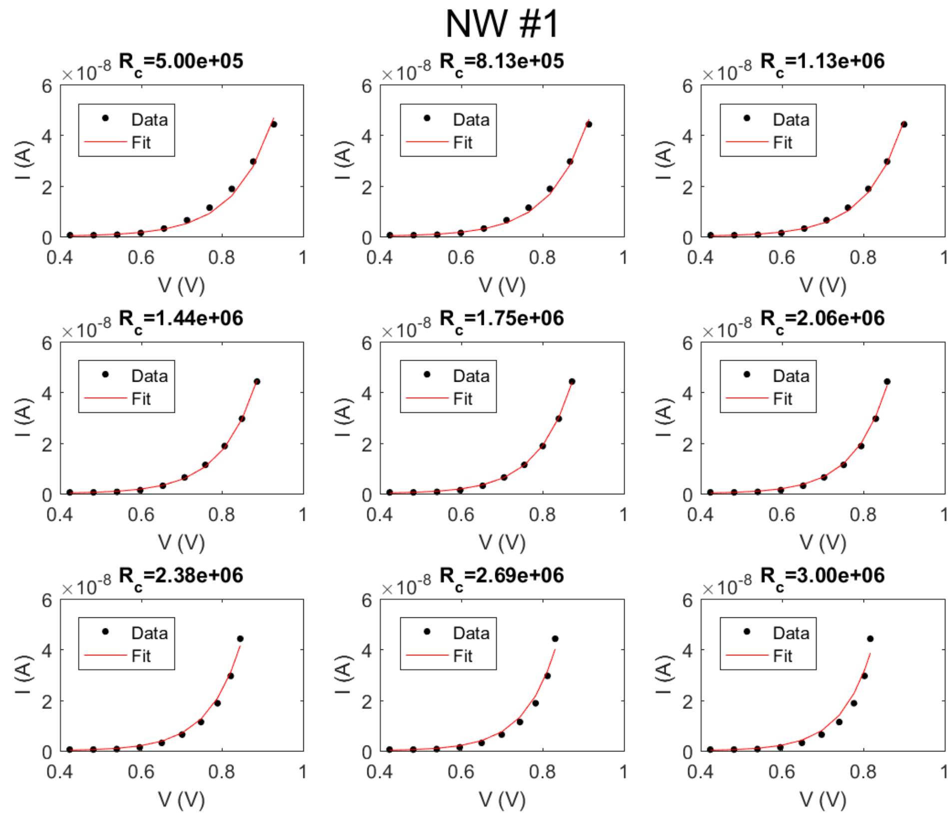

Figure 25: Simulation of the effect of the contact resistance on the excess current for NW #1. Best fit for $R_c = 1.13 \times 10^6$.

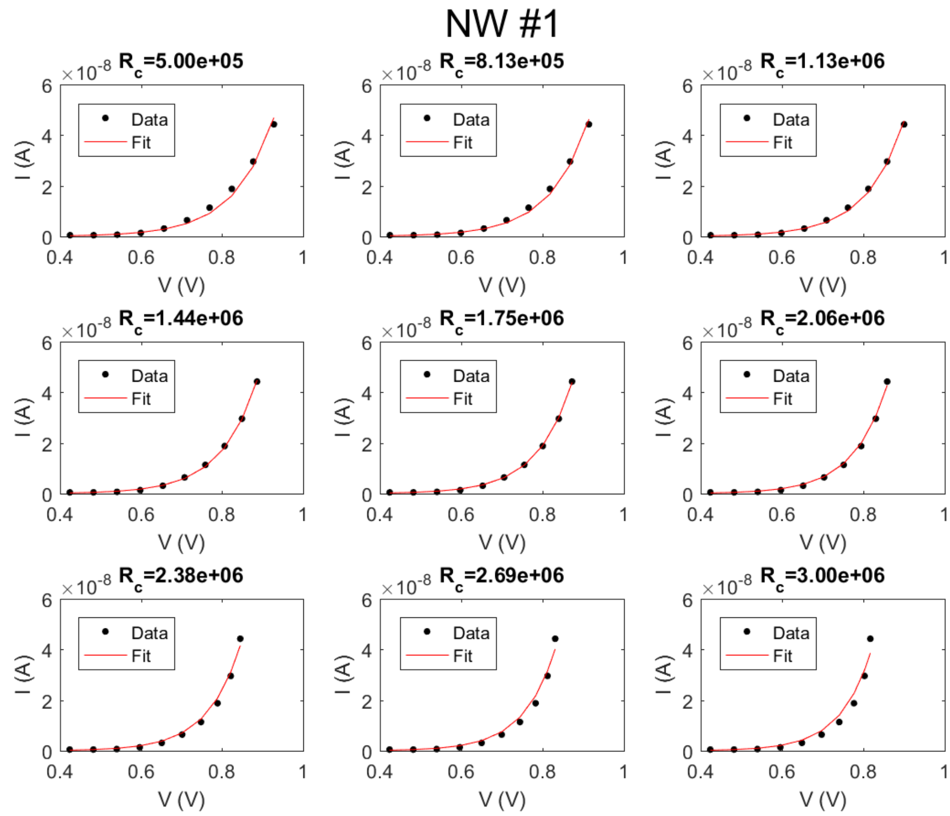

Figure 26: Simulation of the effect of the contact resistance on the excess current for NW #4. Best fit for $R_c = 6.63 \times 10^4$.

Appendix B Matlab code

```
1  function [J] = Current(Ec, Ev, Ef, Na, Nd)
2  % Ec is the conduction band vector
3  % Ev the valence band vector
4  % Ef the Fermi level vector
5  % Na and Nd are the doping levels
6  run('const.m') %physical constants needed
7
8  m=2*(1/m1+1/m2)^-1; %m1=e effective mass, m2=lh effective mass
9  Eg=e*(Ec(end)-Ev(end)-.145); %.145 electron affinity
10
11 EfmEc=Ef(1)-Ec(1);
12 EfmEv=Ef(end)-Ev(end);
13
14 Np=1000;
15 J=zeros(1, Np+1);
16
17 for p=0:Np
18     if Ec(1)+Vm*p/Np>=Ev(end)
19         continue
20     else
21         Efi=sqrt(e*(Ec(end)-Ec(1)-0.145-Vm*p/Np)*Na*Nd...
22                  /(2*eInP*(Na+Nd)));
23         C=180e-9*pi*e^2*Efi/(36*pi*hb^2)*...
24             sqrt(2*m/Eg)*...
25             exp(-4*sqrt(2*m)*Eg^(3/2)/(3*e*hb*Efi));
26         Ebar=sqrt(2/m/Eg)*e*hb*Efi/pi;
27
28         E1=linspace(Vm*p/Np, Ev(end)-Ec(1), 100);
29         E2=linspace(Ev(end)-Ec(1), Vm*p/Np, 100);
30         Es=[E1(1:50) E2(51:100)];
31
32         J(int16(p+1))=C*trapz(E1*e, (F(E1, EfmEc+Vm*p/Np) -...
33             F(E1, EfmEv+Ev(end)-Ec(1))).*(1-exp(-2*Es/Ebar)));
34     end
35 end
36 end
```